applied sciences

MDPI

Article

Optimization of Energy Management Strategy for Series Hybrid Electric Vehicle Equipped with Dual-Mode Combustion Engine Under NVH Constraints

Shupeng Zhang [1], Hongnan Wang [1,*], Chengkai Yang [2], Zeping Ouyang [1] and Xiaoxin Wen [2]

[1] College of Urban Transportation and Logistics, Shenzhen Technology University, Shenzhen 518118, China; zhangshupeng@sztu.edu.cn (S.Z.); ouyangzeping@xiaomi.com (Z.O.)
[2] College of Applied Technology, Shenzhen University, Shenzhen 518060, China; 2310414036@email.szu.edu.cn (C.Y.); 2210414018@email.szu.edu.cn (X.W.)
* Correspondence: wanghongnan@sztu.edu.cn

Abstract: Energy management strategies (EMSs) are a core technology in hybrid electric vehicles (HEVs) and have a significant impact on their fuel economy. Optimal solutions for EMSs in the literature usually focus on improving fuel efficiency by operating the engine within a high efficiency range, without considering the drivability, which is affected by noise–vibration–harshness (NVH) constraints at low vehicle speeds. In this paper, a dual-mode combustion engine was implemented in a plug-in series hybrid electric vehiclethat could operate efficiently either at low loads in homogeneous charge compression ignition (HCCI) mode or at high loads in spark ignition (SI) mode. An equivalent consumption minimization strategy (ECMS) combined with a dual-loop particle swarm optimization (PSO) algorithm was designed to solve the optimal control problem. A MATLAB/Simulink simulation was performed using a well-calibrated model of the target HEV to validate the proposed method, and the results showed that it can achieve a reduction in fuel consumption of around 1.3% to 9.9%, depending on the driving cycle. In addition, the operating power of the battery can be significantly reduced, which benefits the health of the battery. Furthermore, the proposed ECMS-PSO is computationally efficient, which guarantees fast offline optimization and enables real-time applications.

Keywords: hybrid electric vehicle; energy management strategy; homogeneous charge compression ignition; equivalent consumption minimization strategy; particle swarm optimization; NVH constraints

check for updates

Citation: Zhang, S.; Wang, H.; Yang, C.; Ouyang, Z.; Wen, X. Optimization of Energy Management Strategy for Series Hybrid Electric Vehicle Equipped with Dual-Mode Combustion Engine Under NVH Constraints. *Appl. Sci.* **2024**, *14*, 12021. https://doi.org/10.3390/app142412021

Academic Editor: Rodolfo Dufo-López

Received: 1 November 2024
Revised: 14 December 2024
Accepted: 17 December 2024
Published: 22 December 2024

Copyright: © 2024 by the authors. Licensee MDPI, Basel, Switzerland. This article is an open access article distributed under the terms and conditions of the Creative Commons Attribution (CC BY) license (https://creativecommons.org/licenses/by/4.0/).

1. Introduction

Hybrid electric vehicles (HEVs) have become a research focus of the automotive industry, with their technology developing and evolving at a fast pace over the last two decades. They have the potential to reduce fuel consumption and emissions in comparison to conventional vehicles while eliminating the range anxiety issues that electric vehicles (EVs) usually have due to the limited capacity of their battery pack [1,2]. In brief, HEVs combine more than one power source, for example, an internal combustion engine (ICE) and a chemical battery–electric motor. Based on the components' connection and energy flow routes, HEVs can typically be classified as series hybrids, parallel hybrids, series–parallel hybrids, or complex hybrids, and different power sources can be combined through electrical and/or mechanical coupling [3]. In addition, a particular type of HEV called a plug-in hybrid electric vehicle (PHEV) features a large-capacity battery pack, which can be charged from a power grid and covers a certain pure electric driving mileage [4].

The idea behind fuel saving with an HEV is that the ICE can be operated within an efficient range with the assistance of an electric power source. Therefore, the energy management strategy (EMS), which governs the energy distribution between different power sources, becomes the core essential factor of HEV technology [5].

Generally, EMSs can be classified into two main categories: rule-based and optimization-based [6]. For series hybrid electric vehicles (SHEVs), there are two commonly used rule-based EMSs: the thermostat control strategy (TCS) and the power follower control strategy (PFCS). The TCS operates the ICE with a fixed power at the most efficient point, and a state of charge (SOC) fluctuation window is set to determine the engine's on/off status [7]. The TCS can provide the highest engine efficiency. However, the battery's energy loss is relatively large; therefore, the best overall fuel efficiency may not be guaranteed. Furthermore, there is no relationship between engine behavior and driving action, which will result in poor drivability. On the contrary, under the PFCS, the engine output power is made to follow the power demands, and the operation of the battery can be significantly improved. However, the ICE may not always operate within an efficient range; thus, the overall fuel economy could be worse compared to that achieved with the TCS [8]. For PHEVs, since the battery has a relatively large capacity and can achieve zero fuel consumption if the travel distance is shorter than the all-electric range (AER), the charge-depleting–charge-sustaining (CD/CS) strategy, as a rule-based EMS, is widely used. Here, the vehicle uses all-electric energy in the charge-depleting (CD) mode, until the SOC falls below some certain threshold; then, in the charge-sustaining (CS) mode, the SOC is maintained at a relatively stable level by governing the power split between the ICE and the battery [9]. The CD/CS strategy has a simple control logic for real-time implementation; however, its fuel economy is not optimal for long-distance travel [10].

Optimization-based EMSs aim to solve an optimal control problem by minimizing the cost function of fuel consumption and can be classified into two categories: global optimization and real-time optimization. The representative approaches to global optimization include dynamic programming (DP) [11], Pontryagin's minimum principle (PMP) [12], and metaheuristic methods, such as the genetic algorithm (GA) [13] and particle swarm optimization (PSO) [14]. The global optimization method guarantees that the absolute optimal solution will be found, but it is based on the requirement of a priori driving cycle information, and the computational load is fairly high, which makes it unsuitable for real-time implementation. One of the most extensively employed real-time optimization methods is the equivalent consumption minimization strategy (ECMS), which was first proposed by Paganelli [15]. By introducing an equivalent factor (EF), the ECMS transforms electric energy from the battery into an equivalent quantity of fuel consumption and minimizes the total fuel consumption at each instant, which is the sum of the real fuel consumption by the ICE and the weighted equivalent of fuel consumption by the electric motor. Inspired by the PMP [16], the EF can be assumed to be a constant if the battery's SOC remains unchanged; therefore, it is suitable for real-time implementation in PHEVs in charge-sustaining mode. However, the optimal EF is highly dependent on the driving cycle condition, and an EF that is optimal for one particular cycle may be inapplicable to other driving cycles [17,18]. Therefore, various adaptive ECMSs have been proposed to obtain an online-adjusted EF that can be adapted to actual driving conditions: the feedback correction of the EF with respect to target SOC tracking [19], EF correction with look-up tables using the information of vehicle speed and trip length [20], neural network- and learning-based adaption [21], etc. Besides the ECMS, some recent studies have applied the Koopman operator to linearize the high nonlinearities of the powertrain system and combined it with model predictive control (MPC) in a data-driven framework to solve the local optimal problem of EMS [22–24]. This approach reduces the computational complexity and guarantees the real-time optimization of the system; however, it requires sufficient data to train the linearized model to ensure accuracy.

In summary, studies on optimization-based EMSs are largely focused on fuel economy optimization; by including weighted terms in the cost function—such as SOC sustainability, battery health, and ICE start/stop and emissions—a multi-objective optimization problem can be formed to achieve a comprehensive solution for EMSs. However, few studies have considered the noise, vibration, and harshness (NVH) issues that occur with ICEs, which means that the optimized EMS is not applicable in real-world implementations.

Specifically, the NVH of ICEs is relatively high when operating within an efficient range under high loads; it cannot be masked by the road and wind noises if the vehicle is driving slowly. Hence, the ICE should not operate under low vehicle speed conditions, such as in downtown areas or in heavy traffic [25]. However, the battery's SOC is not sustainable if this situation persists for a long time; thus, the ICE has to operate if the SOC has achieved a suitably low threshold, but at a lower load under the NVH constraint. Therefore, the NVH constraint results in a trade-off between fuel economy and SOC sustainability in the charge-sustaining mode.

Homogeneous charge compression ignition (HCCI) combustion is another promising technology for improving fuel economy and reducing emissions that has been widely investigated in recent decades. Compared with conventional spark ignition (SI) combustion, HCCI combustion shows a significant improvement in fuel efficiency under part-load conditions owing to its unthrottled operation, which can reduce pumping loss [26]. However, HCCI combustion has the drawback of a limited operating range due to possible misfire at low loads and knock at high loads. Therefore, in conventional ICE vehicles, it is difficult to operate the engine purely in the HCCI mode; thus, an SI/HCCI dual-mode engine with a mode transition control strategy is required. Furthermore, the combustion timing control and load transition are also challenging due to the auto-ignition mechanism [27].

If we are to retain the advantageous high efficiency under part-load conditions that is achieved with HCCI, as well as the flexibility of power distribution that is achieved with HEVs, then the integration of a dual-mode combustion engine in an HEV is a promising solution. In [28], an SI/HCCI engine was applied in a mild HEV to achieve the torque assist from the integrated starter–generator (ISG), which enables a longer residence time in HCCI combustion. The ECMS supervisory control strategy has shown an improvement of more than 5% in fuel economy for the FTP75 driving cycle in comparison with an SI-only HEV, but barely any improvement was observed for the US06 driving cycle. In [29], dual-mode operation was investigated through a simulation of a power-split HEV equipped with an SI/HCCI engine, and an improvement of 2.5–5% was achieved for fuel consumption. In addition, it led to the prediction of a greater improvement with other types of HEVs, such as parallel architecture HEVs, which have lower flexibility in decoupling engine operations. In [30], a multi-mode low-temperature combustion (LTC) engine—which can operate not only in HCCI mode but also in reactivity-controlled compression ignition (RCCI) mode—was utilized as a range extender for a series HEV. A simulation shows that the multi-mode engine can offer an improvement in fuel consumption of up to 12.1% in comparison with an SI engine for different driving cycles. This is due to the higher engine efficiency in the HCCI mode. Additionally, under the control strategy based on PMP, almost all the operating points of the engine are located in the HCCI and RCCI regions. In [31], different EMSs were investigated for a power-split PHEV integrated with a dual-mode combustion engine, and a hierarchical EMS was proposed to realize the synergy of global and instantaneous optimization. The simulation results show a significant improvement in comparison with the CD/CS strategy for real-world driving cycles. In [32], an adaptive ECMS was developed for a power-split PHEV equipped with a dual-fuel intelligent charge compression ignition (ICCI) engine; this achieved fuel consumption and SOC control performances close to the global optimal results. which were achieved based on DP.

All these studies reveal that the powertrain architecture, the dual-mode engine configuration, hybridization, driving cycle conditions, and EMSs can have an impact on dual-mode engine operation and fuel economy. In this paper, a plug-in SHEV with an SI/HCCI dual-mode combustion engine was investigated, and an EMS based on ECMS was developed to optimize fuel economy in the charge-sustaining mode under NVH constraints. The unique property of series hybrid vehicles is the decoupling of the ICE from the drivetrain, which ensures the convenience of operating the ICE within a limited range and reducing the complexity of HCCI combustion control and SI/HCCI mode transition control. While HCCI combustion has much higher fuel efficiency in comparison with SI combustion in the low-power operating range, it can significantly reduce fuel consumption in urban

driving or heavy traffic, even under NVH constraints. Furthermore, compared with the conventional SI engine, which operates efficiently under high loads or at shutdown, the dual-mode combustion engine enables operation at medium–low power; this is closer to the power demand during driving. Thereby, the battery charging/discharging load is reduced and SOC sustainability is improved, along with benefits for battery health. The key contributions of this article are as follows:

- NVH constraints are considered as the main constraints on engine operating conditions for HEVs; previous studies have usually ignored this. The NVH conditions of the engine have a significant impact on drivability; therefore, they should not be neglected in real-world applications.
- An SI/HCCI dual-mode combustion engine is applied in a SHEV to solve the NVH issue. HCCI combustion enables the high-efficiency operation of the engine at low loads; therefore, this solution guarantees better fuel economy under tight NVH constraints in comparison with SI combustion.
- An EMS based on the ECMS is developed and the optimal control problem is solved by utilizing the PSO algorithm. The fast convergence speed of PSO provides efficient calibration of the control parameters in offline simulations and guarantees online optimization for real-time applications.

This paper is organized as follows. In Section 2, the configuration of the target SHEV and the dual-mode ICE are described, followed by an overview of the proposed control system. The detailed system model and control strategy design based on ECMS combined with PSO are presented in Section 3. The proposed control strategy is validated through simulations for different driving cycles and the results are shown in Section 4. Finally, several conclusions are drawn in Section 5.

2. System Architecture

2.1. Powertrain System Configuration

The SHEV has the simplest structure among all the hybrid powertrain systems, and Figure 1 shows the powertrain structure of the target vehicle, where the black lines and red lines denote the mechanical and electric connections, respectively. The unique characteristic of the SHEV powertrain system is that the engine is mechanically decoupled from the driveline, and it is only used to generate electricity through a generator connected to the engine. In this case, the engine's operating speed is not restricted by the vehicle's speed, and there are opportunities for it to always run at the most efficient points. Since the engine is connected to the generator with a mechanical coupler, the optimal engine speed is controlled by the generator. In this system, the peak power and torque of the generator are designed to be larger than the engine to avoid engine runaway.

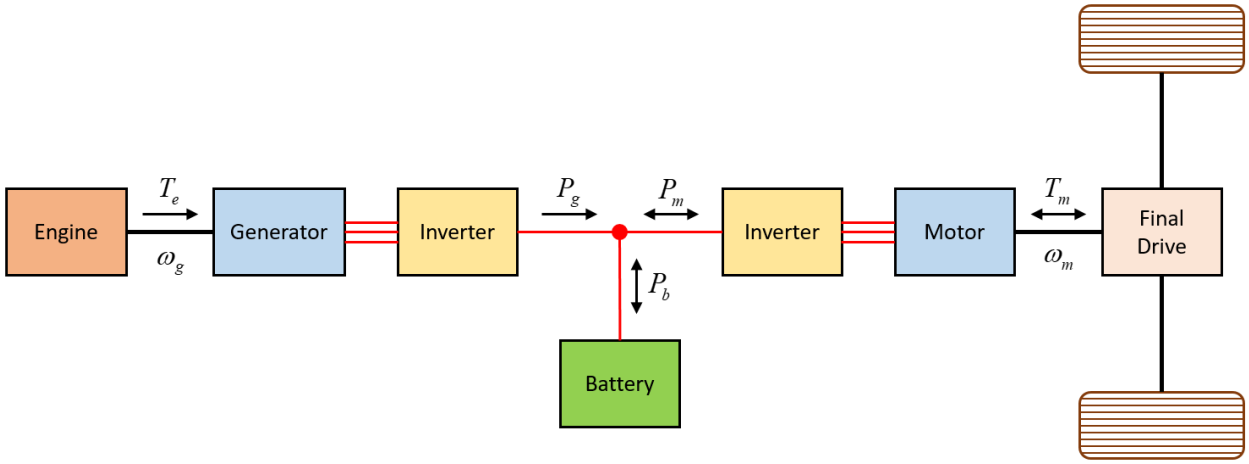


Figure 1. Powertrain structure of the SHEV.

Similar to electric vehicles, a traction motor is the only component that is connected to the driveline, and it provides propulsion in SHEVs. In the target vehicle, the motor is connected to the final drive directly, without the transmission gear box.

Besides the engine–generator set, the battery is the other power source providing electric energy to the motor. For a plug-in SHEV, the battery pack has a relatively large capacity, so that the vehicle has a certain electric driving range, and the battery can act as a "power buffer" to balance the difference between engine–generator output power and the total demanded power. Therefore, the engine has more opportunities to operate within the high efficiency range.

2.2. Dual-Mode Internal Combustion Engine

The internal combustion engine in this powertrain system is an SI/HCCI dual-mode combustion engine for which stable HCCI combustion and SI/HCCI mode transition control was developed in our previous study. It is a 2.0 L, four-cylinder GDI engine equipped with an EVVT system. In the SI combustion mode, the peak power is 125 kW and the maximum torque is 256 Nm. In SHEVs, the internal combustion engine is connected to the generator and the output of the engine–generator set is electric energy instead of mechanical energy; therefore, here, we used the brake-specific fuel consumption (BSFC) map of the whole engine–generator set to interpret the engine's fuel efficiency, and the *y*-axis of the map is chosen to be DC power, as shown in Figure 2. The optimal engine operation curve is shown by the solid red line.

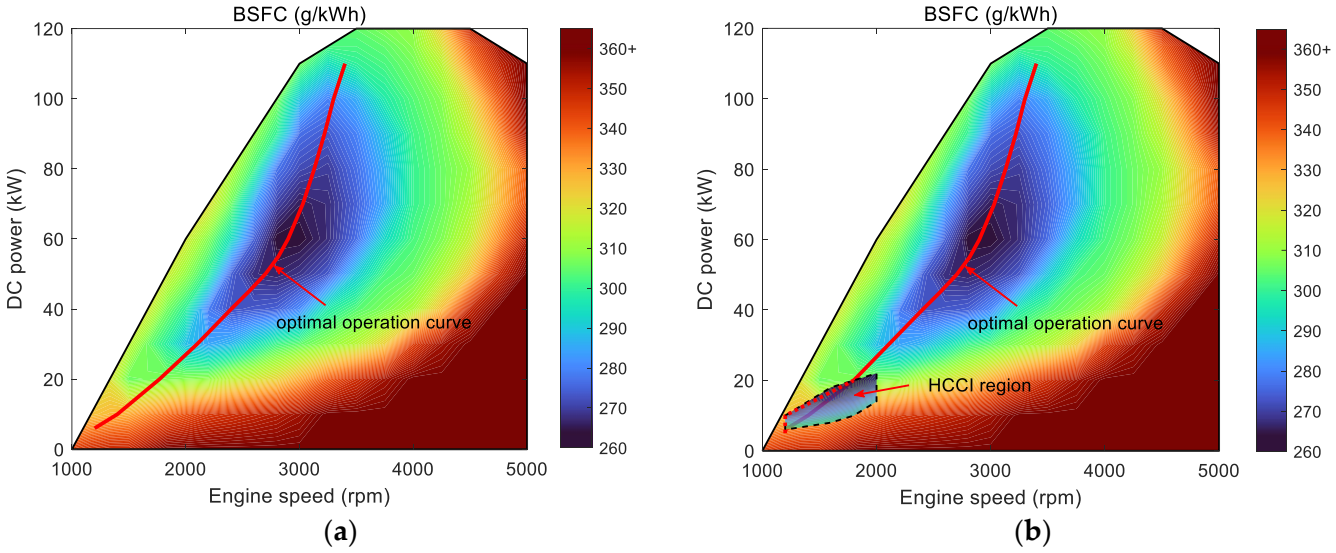


Figure 2. Brake-specific fuel consumption (BSFC) maps of the engine: (**a**) BSFC of the SI combustion engine; (**b**) BSFC of the SI/HCCI dual-mode combustion engine.

Figure 2a shows the BSFC map of the engine-generator set with SI combustion. The optimal operating point of the engine–generator set is at 2900 rpm, 59 kW, with a fuel consumption rate of 263 g/kWh. From the BSFC map, it can be observed that the most efficient range is located around 50 to 80 kW, with speed around 2500 rpm–3200 rpm, where the NVH issue should not be neglected. When the output power is lower than 20 kW, the efficiency drops significantly and the engine should stop operating. Figure 2b shows the BSFC map of the same engine–generator set with dual-mode combustion. The HCCI operating range is relatively small, with a maximum speed of around 2000 rpm and power between 5 kW and 22 kW. The optimal operating point is at 1800 rpm, 20 kW, with a fuel consumption rate of 264 g/kWh. The optimal engine operating curve in HCCI mode is shown by the dashed red line. The two optimal engine operating curves meet at 1800 rpm, 20 kW; thus, this point is chosen as the combustion mode transition point.

Obviously, within the HCCI operating range, the difference in fuel efficiency is more than 20% between the SI mode and the HCCI mode. Therefore, if the engine operates in this range, dual-mode combustion can significantly improve fuel economy.

2.3. Control System Architecture

The control system architecture is shown in Figure 3. This model will be used in control strategy development and simulation validation. The vehicle control unit (VCU) is the supervisory controller in this system. The driver model provides information on driving conditions, such as the demanded power, pedal position, and vehicle speed, and the battery management system (BMS) provides battery information, such as SOC, SOP, internal resistance, and open-circuit voltage, to the VCU for control strategy execution. The VCU runs the ECMS combined with PSO to solve the optimal control solution, which includes the output power of the engine–generator set and the engine combustion mode. Then, based on the BSFC map and the engine's optimal operation curve, the output power signal is split into two control outputs, torque and speed. The torque command will be sent to the engine control unit (ECU), and the speed command will be sent to the generator control unit (GCU). At the same time, the VCU also sends the torque command to the motor control unit (MCU) based on the motor speed feedback. During offline optimization, information on fuel mass flow will be sent to a fuel economy evaluation module to calculate fuel consumption for the purpose of EF optimization by the PSO.

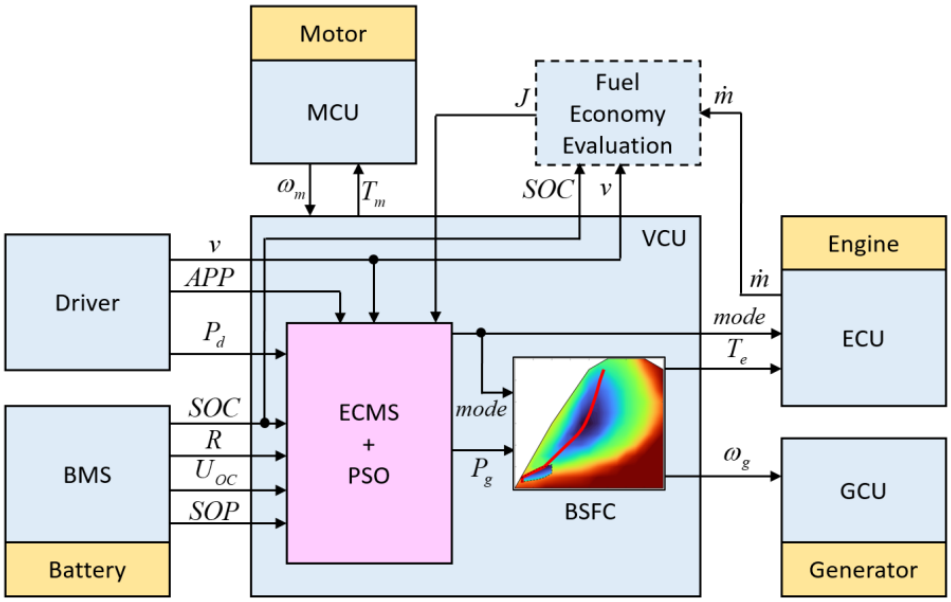


Figure 3. Block diagram of the powertrain control system.

3. Modeling and Control Strategy Design

In this section, a driver model that provides the driving information as the input of the control system and a battery model that provides the battery parameters used for ECMS execution will be presented first. Then, the ECMS problem formulation for the proposed dual-mode engine SHEV powertrain system and the optimization procedure through a dual-loop PSO will be illustrated.

3.1. Driver Model

The driver model generates the load information for any given driving cycle. First, based on the assumption of a road with zero slope, the dynamic equation of the vehicle can be written as:

$$M\frac{dv}{dt} = \frac{T_m i_0 \eta_T}{r} - Mgf - \frac{1}{2}\rho A C_d v^2 \quad (1)$$

On the right-hand side of the equation, the first term represents the traction force, entirely provided by the traction motor; the second term is the rolling resistant force, and the third term is the air drag force. M is the total mass of the vehicle, T_m is the output torque of the motor, i_0 is the gear ratio of the final drive, η_T is the transmission efficiency, r is the radius of the tire, f is the rolling resistance coefficient, ρ is the air density, A is the frontal area of the vehicle, and C_d is the air drag coefficient. Since the traction force is only provided by the motor in SHEVs, the load power is equal to the output power of the motor and can be calculated by:

$$p_{load} = \begin{cases} T_m \omega_m / \eta_m, & T_m \geq 0 \\ T_m \omega_m \eta_m, & T_m < 0 \end{cases} \quad (2)$$

where ω_m is the motor speed and η_m is the motor efficiency. Furthermore, the accessory load under normal driving conditions, such as from air conditioning and infotainment systems, should be considered. Then, the total required power is obtained by:

$$p_d = p_{load} + p_{acc} \quad (3)$$

Second, the drive model aims to simulate the actual driving actions; that is, the driver uses the accelerator/brake pedals to control the traction torque based on the vehicle speed. In this model, a PI controller is designed to generate the desired pedal position signal according to the vehicle's speed tracking error. Note that the accelerator pedal's position signal and brake pedal's position signal are combined together and denoted by *APP*, where the brake pedal's position is defined by a negative value for convenience. Then, a pre-calibrated map converts the pedal position to the desired torque at different vehicle speeds. The torque signal will be sent to the dynamic equations of the vehicle to obtain the instantaneous speed and complete the feedback loop. The structure of the closed-loop driver model is shown in Figure 4. The outputs of the driver model include the total required power, which will be used for the ECM decision, and the vehicle speed and APP information, which will be used as NVH constraints.

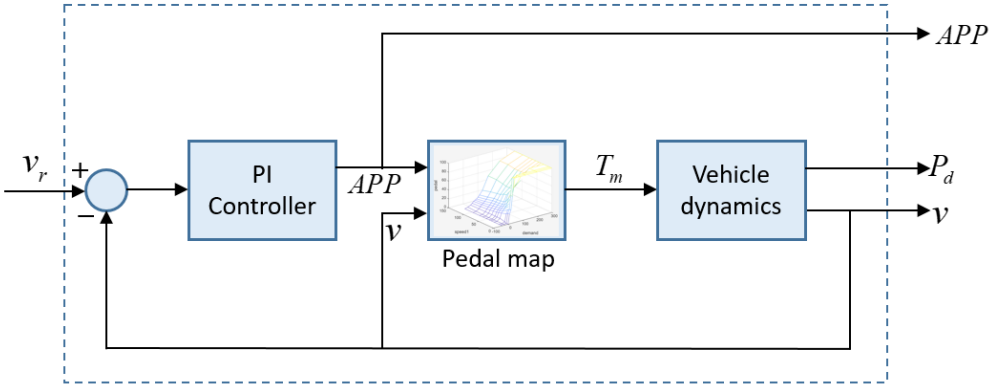


Figure 4. Closed-loop driver model.

3.2. Battery Model

The battery model calculates the instantaneous SOC of the battery pack and provides the other parameters required by the energy management control strategy, such as the open-circuit voltage, the internal resistance, and the SOP of the battery. For the convenience of control implementation, the Rint model is chosen instead of the equivalent circuit model with several RC circuits, and the model in shown in Figure 5.

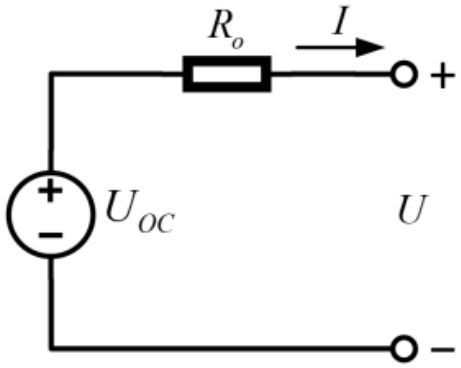


Figure 5. Rint model of the battery.

The Rint model consists of a voltage source reflecting the open-circuit voltage of the battery, and a resistor representing the internal resistance of the battery. When the battery is discharging, the output voltage will be lower than the open-circuit voltage because the voltage drops on R. Similarly, the output voltage will be higher than the open-circuit voltage when the battery is charging. By defining a positive value for the current when discharging, the output power of the battery can be calculated by:

$$p_b = UI = (U_{OC} - IR)I \tag{4}$$

By solving this equation, the output current of the battery can be obtained as shown in Equation (5).

$$I = \frac{U_{OC} - \sqrt{U_{OC}^2 - 4Rp_b}}{2R} \tag{5}$$

In this equation, the open-circuit voltage, U_{OC}, is a function of SOC, which is experimentally calibrated and stored as a lookup table in the model. The internal resistance, R, is a function of both the temperature and the SOC, which is also calibrated through battery charge/discharge tests and stored as a 2D lookup table in the model.

Normally, the battery capacity is defined in the unit of Ah; SOC can be calculated by the ampere-hour integral method, as shown in Equation (6):

$$SOC = SOC_0 - \frac{1}{C_b}\int \eta_C I(t)dt \tag{6}$$

where SOC_0 is the initial SOC, C_b is the total capacity of the battery, and η_C is the Coulomb efficiency of the battery. The physical interpretation of Coulomb efficiency shows that η_C depends on the temperature and charge/discharge rate, and it is difficult to obtain an accurate value at every moment. Therefore, in this study, we calculate SOC based on energy:

$$SOC = SOC_0 - \frac{1}{E_b}\int U_{OC}(t)I(t)dt \tag{7}$$

where E_b is the total energy when the battery is fully charged. The integral term is the total power of the battery, including output power and the Joule heat power generated by the battery's internal resistance, by taking the open-circuit voltage instead of output voltage as the integrated part.

Finally, the battery model should provide the SOP information, which includes the maximum discharge power and maximum charge power. In the same way as for the current, we define the maximum discharge power with a positive value denoted by $p_{b\max}$, and the maximum charge power is defined with a negative value, denoted by $p_{b\min}$. Both values are SOC- and temperature-dependent, and they are stored in the model as 2D lookup tables.

3.3. ECMS Problem Formulation

3.3.1. Equivalent Consumption Minimization Strategy

For SHEVs with the powertrain structure shown in Figure 1, the power balance equation can be written as:

$$p_d(t) = p_g(t) + p_b(t) \tag{8}$$

where p_g is the output power of the engine–generator set. Combing Equations (5), (7), and (8), the dynamics of the powertrain energy system can be written as a differential equation for SOC, as shown in Equation (9):

$$\dot{SOC} = \frac{U_{OC}^2(t) - U_{OC}(t)\sqrt{U_{OC}^2(t) - 4R(t)\left(p_d(t) - p_g(t)\right)}}{2R(t)} \tag{9}$$

and it can be further represented in a state space form:

$$\dot{x}(t) = f(x(t), u(t)) \tag{10}$$

where the state, x, is the battery SOC; the control input, u, is the output power of the engine–generator set, which is p_g in Equation (9). The battery open-circuit voltage and resistance are SOC-related; therefore, the right-hand side of Equation (9) can be represented by a function of state and input. In general, the constraints for the state and the control variables include:

$$\begin{cases} SOC_{\min} \le SOC \le SOC_{\max} \\ 0 \le p_g(t) \le p_{g\max} \\ p_{b\min}(t) \le p_b(t) \le p_{b\max}(t) \end{cases} \tag{11}$$

where the state-variable SOC is constrained within a narrow window in the charge-sustaining mode and the width of $[SOC_{\min}, SOC_{\max}]$ is chosen to be 5% in this study; the engine–generator set's output power is limited by $p_{g\max}$; this is 120 kW in this study according to $p_{e\max}$, as defined in Table 1 along with the generator efficiency; the battery output power is constrained by the instantaneous SOP, which was discussed in Section 3.2.

Table 1. Main parameters of the target SHEV.

Component	Parameter	Notation	Value
Vehicle	Total mass	M	2040 (kg)
	Final drive/gear ratio	i_0	4.2
	Radius of the tire	r	0.371 (m)
	Frontal area	A	2.1 (m^2)
	Rolling resistance coefficient	f	0.0098
	Air drag force coefficient	C_d	0.28
Engine	Peak power	$p_{e\max}$	125 (kW)
	Maximum speed	$\omega_{e\max}$	5000 (rpm)
	Maximum torque	$T_{e\max}$	256 (Nm)
Motor	Peak power	$p_{m\max}$	300 (kW)
	Maximum speed	$\omega_{m\max}$	6000 (rpm)
	Maximum torque	$T_{m\max}$	1340 (Nm)
Battery pack	Total capacity	E_b	19.7 (kWh)
	Nominal voltage	U_b	346.5 (V)

Then, the optimal control of fuel economy can have a cost function in the general form of:

$$J = \int_{t_0}^{t_f} \dot{m}_{fuel}(u(t), t)dt \tag{12}$$

where the control input is the same as p_g in the state equation. When operating in the charge-sustaining mode, the total consumed energy from the battery is negligible; hence, the battery is acting as an auxiliary reversible fuel tank: if the engine's output power is higher than the required power, with extra power to charge the battery, the charged energy will be released in the future and fuel will be "saved"; if the engine's output power is lower than the required power, the battery discharges at this moment and needs to be recharged in the future to "consume" the fuel. Based on this mechanism, the ECMS introduces an equivalent factor (EF) to transform electric energy into an equivalent amount of fuel, and the global optimization problem is converted to a local optimization problem with a cost function in the form of:

$$\dot{m}_{eqv}(t) = \dot{m}_{fuel}(t) + s(t)\dot{m}_{elec} = \dot{m}_{fuel}(t) + s(t)\frac{p_b(t)}{Q_{LHV}} \tag{13}$$

where m_{eqv} is the equivalent fuel consumption rate; m_{elec} is the converted equivalent fuel consumption from electric energy, which is equal to the battery power divided by the fuel low heating value; and s is the equivalent factor.

The theoretical inspiration for ECMS is the global optimization approach by Pontryagin's minimum principle (PMP). The Hamiltonian function for the global optimal control problem described in Equation (12) can be written as:

$$H(x(t), \lambda(t), u(t), t) = \dot{m}_{fuel}(u(t), t) + \lambda(t)\dot{x}(t) \tag{14}$$

where the state, x, is the battery SOC, the control input, u, is the engine power, and λ is the co-state. If we define an EF "s" by

$$s(t) = -\lambda(t)\frac{Q_{LHV}}{U_{OC}(SOC)C_b}, \tag{15}$$

then Equation (14) can be converted to Equation (13). Based on the PMP, the equation of the co-state derived from the Hamiltonian function can be written as:

$$\dot{\lambda}(t) = -\frac{\partial \dot{m}_{fuel}(u(t), t)}{\partial x} - \lambda(t)\frac{\partial f(x(t), u(t))}{\partial x} \tag{16}$$

The battery's open-circuit voltage and resistance are SOC-dependent; however, usually, the variation is small, especially in the charge-sustaining mode where the SOC is maintained in a narrow range. Therefore, the right-hand side of Equation (16) is approximately zero, which implies that the co-state can also be treated as a constant [1]. This assumption was also validated through global optimization results [33]. Based on the equivalence between PMP and ECMS discussed above and Equation (15), the EF of ECMS can also be approximated by a constant. However, the charge/discharge efficiency should be considered due to the energy loss on the battery's internal resistance, and the commonly used method is to define the EF by two separated values [18]:

$$\begin{cases} s_{chg} = s \cdot \eta_b \\ s_{dis} = s/\eta_b \end{cases} \tag{17}$$

The problem is that the charge/discharge efficiency η_b is not constant and depends on many factors, such as cell temperature, SOC, and charge/discharge rate. Therefore, using an average value of efficiency will lead to inaccuracies. In this study, we considered the actual electrochemical power taken out of or stored in the battery instead of the output power and combined the two cases into one. That is, we replace the output power, P_b, in Equation (13) with P_{ech}, which is the battery current multiplied by the open-circuit voltage:

$$p_{ech} = U_{OC}I = \frac{U_{OC}^2 - U_{OC}\sqrt{U_{OC}^2 - 4Rp_b}}{2R} \tag{18}$$

Then, the ECMS cost function becomes:

$$\dot{m}_{eqv}(t) = \dot{m}_{fuel}\left(p_g(t), t\right) + s(t)\frac{U_{OC}^2(t) - U_{OC}(t)\sqrt{U_{OC}^2(t) - 4R(t)\left(p_d(t) - p_g(t)\right)}}{2Q_{LHV}R(t)} \quad (19)$$

where the battery's instantaneous open-circuit voltage, U_{OC}, and the internal resistance, R, will be obtained from the battery model. It is subject to the following constraints:

$$\begin{cases} p_{g\min}(t) \le p_g(t) \le p_{g\max}(t) \\ p_g(t) \le p_{NVH}(t) \\ p_{b\min}(t) \le p_b(t) \le p_{b\max}(t) \\ p_d(t) - p_{b\max}(t) \le p_g(t) \le p_d(t) - p_{b\min}(t) \end{cases} \quad (20)$$

where the first constraint shows the operating range of the engine–generator set in different combustion modes; the second constraint is an NVH constraint, considering the drivability, which will be illustrated in the next subsection; the third constraint gives the battery's operating range and this will restrict p_g at different driving loads, as shown by the fourth constraint. Combining these four constraints together, the final constraint on the control input, p_g, can be derived as:

$$p_{\min}(t) \le p_g(t) \le p_{\max}(t) \quad (21)$$

where

$$\begin{cases} p_{\min} = \max\left(p_d(t) - p_{b\max}(t),\ p_{g\min}(t)\right) \\ p_{\max} = \min\left(p_d(t) - p_{b\min}(t),\ p_{g\max}(t),\ p_{NVH}(t)\right) \end{cases} \quad (22)$$

In order to maintain a relatively stable SOC, an SOC-based feedback control is designed to adjust the value of EF based on the SOC tracking error:

$$s(t) = \alpha\left(1 + \beta\left(SOC(t) - SOC_{ref}\right)\right) \quad (23)$$

where α is the nominal value of EF, β is the proportional gain of the SOC tracking error, and SOC_{ref} is the reference SOC to sustain. With given values of α and β, the optimal control can be solved:

$$p_g^*(t) = \arg\min_{p_g(t) \in [p_{\min},\ p_{\max}]}\left(\dot{m}_{eqv}\left(p_g(t), p_d(t), s(t), t\right)\right) \quad (24)$$

Furthermore, based on the solved optimal output power of the engine–generator set, the engine combustion mode can be determined by checking whether $p_g^*(t)$ is located within the HCCI operation range or the SI operation range.

Note that the battery parameters, such as SOC, SOP, and resistance, cannot be measured accurately. It will have an impact on the optimization results, as can be seen from Equation (19). Take the resistance, R, as an example: if it is overestimated, then the battery loss will also be overestimated, leading to less usage of the battery and more deviation from the optimal operating point of the engine; on the contrary, if R is underestimated, then the engine will have more opportunity to operate at the most efficient point, which is similar to the thermostat strategy. In the simulation, these parameters are obtained from pre-stored lookup tables and assumed to be accurate. In real applications, these parameters will be estimated by an advanced algorithm, such as the extended Kalman filter (EKF), to guarantee sufficient accuracy. Since this is not the focus of this study, the details will be omitted here.

3.3.2. NVH Constraint

In SHEVs, the engine is decoupled from the drivetrain; ideally, it can operate at any power and speed, and there is no direct relation between the engine's operating condition

and the vehicle's driving condition. Based on the optimal control strategy, which only considers the fuel economy, it is quite possible that the engine will run at high loads when the vehicle speed is low or the required power is low. This brings in an NVH issue and results in relatively bad drivability.

In this study, an NVH constraint is set to limit the engine–generator set's output power at different vehicle speeds and pedal positions. The maximum allowed power, p_{NVH}, under different driving conditions was calibrated during real-world driving based on the driver's intentions. The values of p_{NVH} are shown in Figure 6. When the vehicle speed is low, p_{NVH} is also relatively low; however, as the driver presses the accelerator pedal harder, higher power is subjectively expected; thus, the constraint is looser. As the vehicle's speed increases, wind and road noise increasingly suppress the engine noise; therefore, a larger p_{NVH} is allowed at a higher vehicle speed.

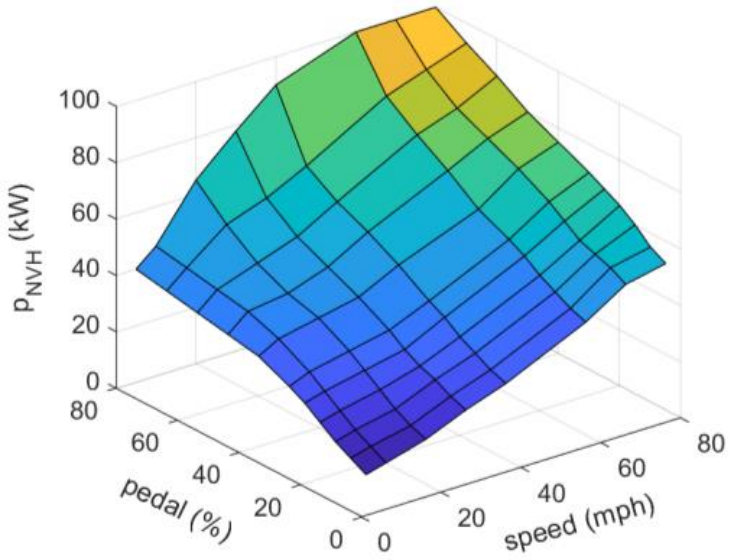


Figure 6. Map of NVH constraints on the engine–generator set's output power.

3.3.3. Engine Operating Range

The other issue related to drivability is the engine's frequent on/off and frequent mode switches between SI and HCCI. These phenomena are mainly a result of the fact that the ECMS only optimizes the fuel economy by minimizing the cost function of the equivalent mass flow rate at each instant without considering the engine's operational condition switches within a period of time. To solve this problem, a hysteresis of engine operation is set to reduce the condition switch.

The whole logic of engine operating range determination is shown in Figure 7. In detail, for SI combustion mode operation, a minimum engine-on time (such as 5 s) is defined; once the engine starts, it cannot be shut down until this requirement is satisfied. For SI/HCCI dual-combustion-mode operation, both the minimum SI operation time and the minimum HCCI operation time are defined (both are 5 s in this study); the engine is not allowed to switch modes unless it has stayed in the current mode for longer than 5 s. Based on this strategy, the engine operating range can be determined; that is, the values of $p_{g\max}$ and $p_{g\min}$ in Equation (20) are determined. If there is no restriction in the next moment, then the engine can operate within 0 kW–120 kW; 0 kW means the engine is off. If the engine must operate in the HCCI mode, then the operating range is between 5 kW and 20 kW; although the maximum power in the HCCI mode is 22 kW, in order to switch to the SI mode on the engine's optimal operation curve smoothly, the maximum operating point is chosen to be 20 kW at 1800 rpm. If the engine must operate in the SI mode, then the operating range is between 5 kW and 120 kW; below 20 kW, the engine should operate along the optimal BSFC curve in the SI mode instead of the HCCI mode, and the minimum

power is chosen to be 5 kW instead of 0 kW. This is because the lowest NVH-constrained power is 5 kW and there is no reason for the engine to operate below this value.

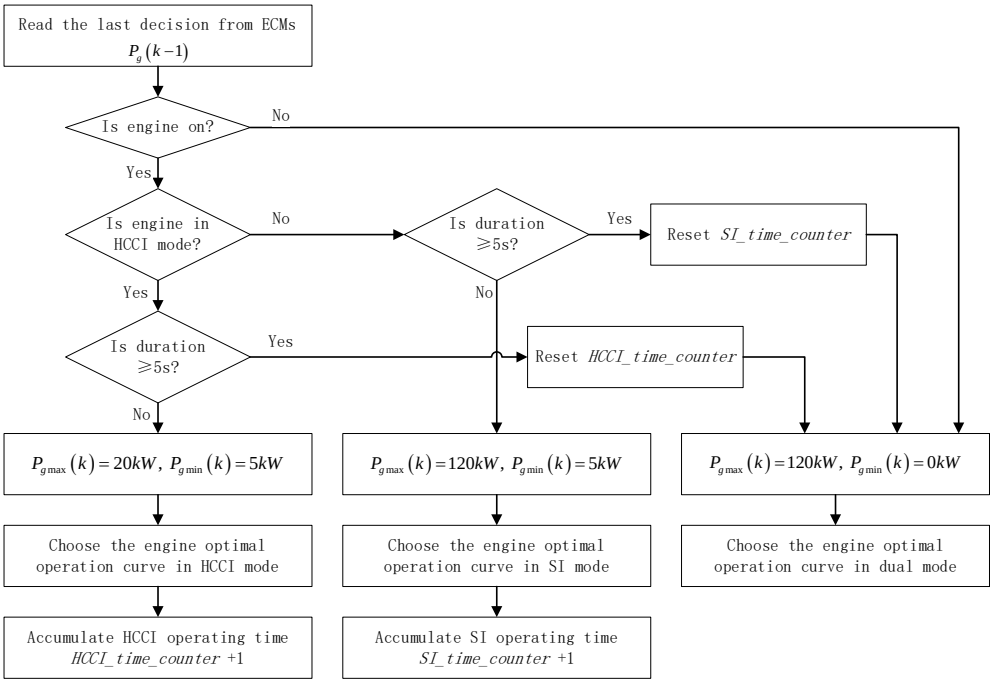


Figure 7. Determination of the engine's operating range in different combustion modes.

3.4. Optimization with the PSO Algorithm

The optimization target is to minimize fuel consumption during a given driving cycle. Furthermore, for an SHEV driving in charge-sustaining mode, the ΔSOC between the start and the end of the cycle and the SOC fluctuations during the cycle should also be considered. Therefore, the cost function of evaluating the overall fuel economy can be written as:

$$J = \int_{t_0}^{t_f} \dot{m}_{fuel}(t)dt + W_1 \int_{t_0}^{t_f} \left(SOC(t) - SOC_{ref}\right)^2 dt + W_2 \left(SOC\left(t_f\right) - SOC_{ref}\right)^2 \quad (25)$$

where the first term on the right side of the equation denotes the total fuel consumption during the whole driving cycle, the second term is the penalty of SOC fluctuations, and the third term is the penalty of SOC deviations at the end of the driving cycle. W_1 and W_2 are the weightings. Based on the theory of ECMS, this global optimization problem can be converted to a local optimization problem where only the instantaneous equivalent fuel consumption is required to be minimized, which is illustrated by Equations (19) and (24); therefore, the online optimization is applicable.

The EF plays an essential role in ECMS; however, it heavily depends on the driving cycle. An optimal EF for one particular driving cycle may not achieve optimal results for another one. Moreover, with multiple constraints and time-varying parameters, it is fairly difficult to obtain an analytical solution for this optimization problem. Therefore, in this study, PSO, a heuristic optimization algorithm, is adopted to search for an optimal solution.

Inspired by the social behavior of bird flocking and fish schooling, the basic idea of solving an optimal control problem using PSO is that the candidate solution can be represented by particles; during the iteration, each particle updates the velocity and position according to the global best and personal best based on evaluating the fitness values obtained by the particle swarm. The iterative law can be written as

$$v^i(k+1) = wv^i(k) + c_1 r_1 \left(P^i_{best} - x^i(k)\right) + c_2 r_2 \left(G_{best} - x^i(k)\right) \quad (26)$$

$$x^i(k+1) = x^i(k) + v^i(k+1) \tag{27}$$

where $v^i(k)$ is the velocity of the ith particle at the kth iteration; $x^i(k)$ is the position of the ith particle at the kth iteration; P^i_{best} is the personal best position of the ith particle; G_{best} is the global best position of all the particles; w is the inertia weight; c_1 and c_2 are learning factors, which are two constants between 0 and 2; and r_1 and r_2 are uniform random numbers between 0 and 1. Once the stopping criteria are satisfied (e.g., the maximum iteration number is achieved), the iteration will be ended and the global best, along with the corresponding optimal particle position, can be determined.

In this study, in order to optimize the EF and solve the ECMS problem for a given driving cycle, a dual-loop PSO algorithm is adopted, as shown in Figure 8. The outer loop (see Figure 8a) is used to find out the optimal EF for ECMS, and each particle is a two-dimensional vector that represents the two parameters, α and β, in EF, as defined by Equation (23). With a fixed EF, the ECMS problem for a given driving cycle becomes solving the optimal control problem defined by Equation (24) at each time step of the cycle. Therefore, the inner loop of PSO (see Figure 8b) is used to find out the optimal $p^*_g(t)$. For offline optimization, the dual-loop PSO algorithm operates as follows:

1. Run the outer loop PSO. Each particle is a candidate solution of EF containing two parameters. The fitness function is defined in Equation (25).
2. At the beginning of one iteration, the position of a particle is fixed and the corresponding EF can be determined.
3. The Simulink model will be called and the driving cycle will be run from the beginning to the end with the given EF. The inner loop PSO is executed to solve the ECMS at each time step. The fitness function of a particle is defined in Equation (19), with constraints defined in Equation (21).
4. After the simulation of the whole cycle is ended, the fitness function of each particle in the outer loop PSO will be evaluated and the iteration continues until the stopping criteria are satisfied.

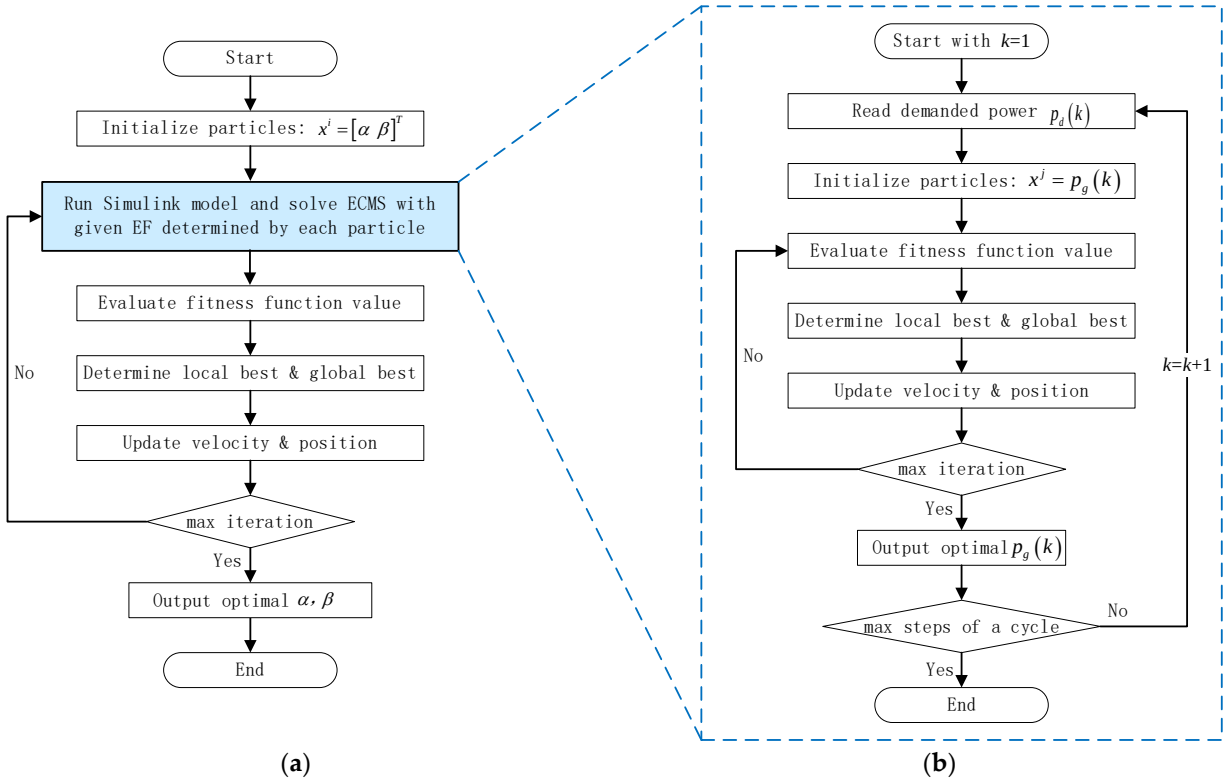


Figure 8. Dual-loop PSO algorithm: (**a**) the outer loop of the PSO algorithm searches for the optimal EF; (**b**) the inner loop of the PSO algorithm solves the ECMS problem at each instant.

For online applications, since the driving cycle information is unknown, the EF will be fixed after offline optimization and only a single-loop PSO is applied to solve the ECMS problem.

4. Results and Discussion

To evaluate the fuel economy of the proposed control strategy along with the dual-mode engine, six standard driving cycles were selected for simulation validation, as shown in Figure 9. Among those driving cycles, the UDDS cycle represents urban driving conditions and contains a period of medium–high-speed driving; the HWFET cycle represents highway driving without any stops; the MANHATTAN cycle and NYCC cycle represent low-speed urban driving with traffic and frequent start/stops; the US06 cycle represents aggressive driving behavior with high speed and high acceleration; and the WLTC cycle is a comprehensive driving cycle containing multiple driving conditions and covering a large range of vehicle speeds.

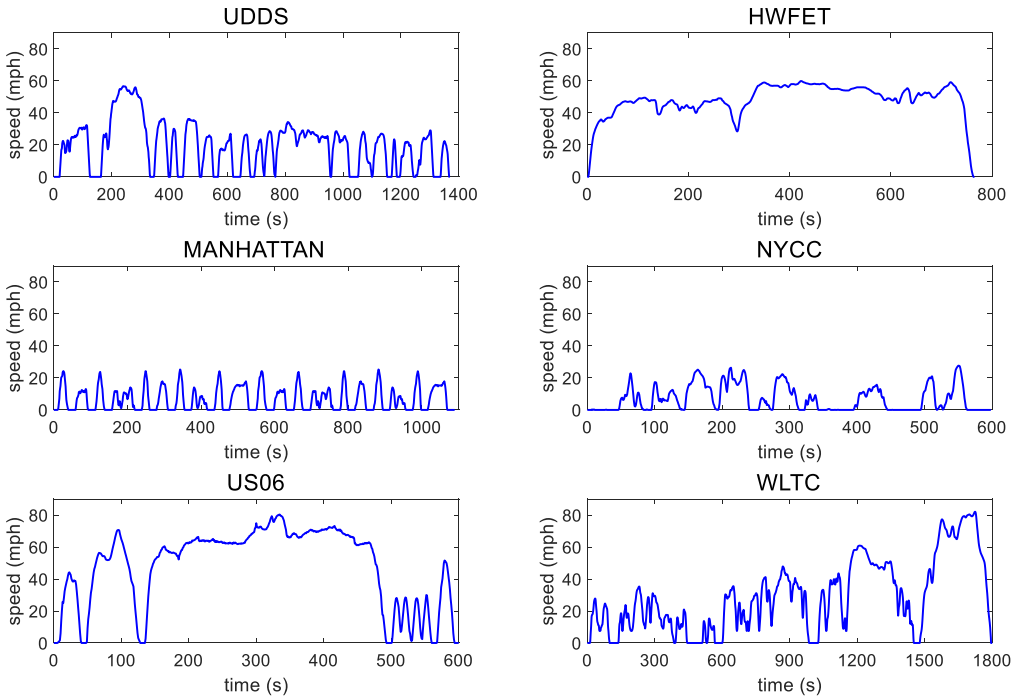


Figure 9. Standard driving cycles for simulations in this study.

The simulation was performed on a personal computer with Intel Core) i7-10710U CPU@1.10GHz, in a MATLAB/Simulink (R2024a) environment with a well-calibrated model of the target SHEV powertrain system. The simulation was divided into two steps:

Step 1: Offline calibration—the first five driving cycles were conducted in the simulation with the dual-loop PSO algorithm to find the optimal EFs for different driving conditions; the average iteration time for each driving cycle is around 112 min.

Step 2: Online validation—the WLTC cycle was used to evaluate the control performance when the EF was fixed after optimization and a single-loop PSO algorithm was applied to solve the ECMS problem; the calculation was finished within 70 s, which is less than 4% of the cycle duration of 1800 s, which shows that the PSO algorithm fulfills the requirement of real-time implementation.

In order to investigate the impact of driving conditions on the optimal EF, and to evaluate the benefit of dual-mode engine operation, three strategies were applied in the simulation for comparison. The results are shown in Table 2.

Table 2. Comparison of fuel economy and optimal EF between different strategies.

Cycle	Strategy	α	β	MPG	Improvement (%)	max ΔSOC	Engine On/Off
UDDS	SI w/o NVH	3.26	0.05	48.63		0.86	179
	SI w/NVH	3.52	0.156	45.9		4.05	26
	SI/HCCI	3.2	0.022	48.84	5.0	0.64	59
HWFET	SI w/o NVH	3.2	0.026	43.7		1.38	142
	SI w/NVH	3.27	0.023	42.43		1.37	43
	SI/HCCI	3.19	0.024	44.28	3.1	0.9	27
MANHATTAN	SI w/o NVH	3.27	0.025	36.95		0.45	18
	SI w/NVH	3.68	0.021	33.31		0.25	14
	SI/HCCI	3.22	0.02	37.04	9.9	0.24	25
NYCC	SI w/o NVH	3.26	0.026	37.14		0.54	14
	SI w/NVH	3.56	0.022	33.96		0.35	11
	SI/HCCI	3.21	0.02	37.23	8.8	0.18	16
US06	SI w/o NVH	3.12	0.035	37.29		2.1	77
	SI w/NVH	3.16	0.027	36.44		1.48	42
	SI/HCCI	3.14	0.042	37.06	1.3	1.64	33

- Strategy 1: SI combustion without NVH constraints. Under this strategy, the internal combustion engine will only operate in the SI mode. The instantaneous engine power is determined by the optimal ECMS solution without NVH constraints. This is the ideal case, which could achieve the optimal fuel economy for SI mode operation.
- Strategy 2: SI combustion with NVH constraints. NVH constraints will be considered in this case, including the maximum allowed engine power due to NVH and the minimum engine-on time to avoid frequent engine on/off switching. Under this strategy, the engine could operate away from the efficient range under some of the driving conditions; therefore, the fuel economy will be worse than in Strategy 1. This strategy will also be considered as a baseline for comparison with Strategy 3.
- Strategy 3: SI/HCCI dual-mode combustion with NVH constraints. This is the proposed strategy in this study. The internal combustion engine can operate in either SI or HCCI modes depending on the optimization result, and multiple NVH constraints are applied. This allows certain assessments, e.g., considering the maximum allowed power at low speed or low load, and avoiding frequent engine start/stop and frequent mode switches.

ECMS combined with PSO is applied in each strategy to determine the engine on/off status and engine–generator output power. For the purpose of investigating the benefit of the dual-mode combustion engine in an SHEV in the charge-sustaining mode with NVH constraints, the other energy management strategies, such as thermostat and power follower, are not considered for comparison in this study.

By choosing a proper weighting in Equation (24), all the cases have achieved a minimum SOC deviation by the end of the cycle; thus, it is fair to evaluate the fuel economy by MPG (miles per gallon). It can be seen that Strategy 3—which applies dual-mode combustion—can achieve a higher MPG for all the simulated driving cycles than Strategy 2; this is roughly the same as that achieved in Strategy 1. Among those cycles, dual-mode combustion can bring the largest benefit in the MANHATTAN cycle and the NYCC cycle, and the MPG improvement is around 9–10 percent compared with single SI mode combustion. The main reason is that for cycles with traffic, the engine's output power is limited by NVH constraints and the engine's operation is not in the efficient range, while HCCI combustion could have high efficiency under those conditions. Furthermore, Strategy 3 has minimal SOC fluctuations and relatively lower engine start times. Strategy 1 has the most frequent engine on/off switches due to the deficiency of hysteresis.

From the aspect of the optimal EF parameters α and β, it is obvious that they are driving-cycle-dependent for all strategies. In other words, they are sensitive to the driving

conditions, and in Strategy 2, they have the highest sensitivity. In detail, α is relatively larger in higher speed cycles, and β could vary significantly since it is required to reduce SOC fluctuations. However, in Strategy 3, both α and β do not vary too much between different driving cycles, which can guarantee better robustness in real-time applications, since the load condition is usually unknown during real-world driving.

To further investigate the improvement in fuel economy achieved by the dual-mode combustion engine, more data reflecting the engine and battery performance, such as the average BSFC and battery loss, were recorded as shown in Table 3.

Table 3. Comparison of engine and battery performances between different strategies.

Cycle	Strategy	Avg. BSFC (g/kWh)	Engine–Generator Set Total Work (kWh)	Battery Loss (kWh)	Avg. Battery Power (kW)
UDDS	SI w/o NVH	263	2.017	0.0533	10.14
	SI w/NVH	278.48	2.007	0.0411	9.32
	SI/HCCI	264.5	1.986	0.0233	6.48
HWFET	SI w/o NVH	263	3.072	0.0698	18.63
	SI w/NVH	272.91	3.049	0.0425	15.15
	SI/HCCI	264.52	3.016	0.0107	5.47
MANHATTAN	SI w/o NVH	263	0.732	0.0189	5.74
	SI w/NVH	294.08	0.726	0.0092	4.51
	SI/HCCI	264.97	0.725	0.0085	4.34
NYCC	SI w/o NVH	263	0.416	0.0109	5.81
	SI w/NVH	291.05	0.411	0.0069	4.81
	SI/HCCI	265.47	0.411	0.0067	4.69
US06	SI w/o NVH	263	2.812	0.0735	19.64
	SI w/NVH	268.81	2.815	0.0753	19.81
	SI/HCCI	265.23	2.807	0.0726	17.98

It can be seen that, under Strategy 1, the average BSFC of the engine is a constant for all the driving cycles, which is the global optimal value that the engine can achieve within the whole BSFC map. This is similar to the "thermostat" strategy, which also operates the engine at a fixed optimal point; however, the engine on/off algorithm is different between thermostat and Strategy 1, which results in a better fuel economy by applying ECMS, and the comparison is omitted here. With Strategy 2, the engine's output power is limited by the NVH constraint; thus, the achieved average BSFC was higher than the global optimum. Furthermore, in the MANHATTAN and NYCC cycles, the average BSFC is significantly higher than in the other strategies; this can explain the much lower MPG for these cycles under Strategy 2 in Table 2.

With SI/HCCI dual-mode combustion, the engine will not always operate at the global optimal point which is in the SI combustion region. Therefore, the average BSFC of a cycle under Strategy 3 is lower than it is under Strategy 1. However, from Table 2, it can be seen that, in most of the cycles, Strategy 3 can achieve an even higher MPG than Strategy 1. The reason is that, under SI/HCCI combustion, the gap between the engine–generator set's output power and the required power for driving is greatly narrowed (since the optimal operating range of the engine in SI mode is at high loads) and the average battery power is lowered; thereby, the battery loss due to the internal resistance is reduced. Then, based on energy conservation, the total work of the engine–generator set for a certain driving cycle is lower than that which has higher battery loss.

From Table 2, we can see a decrease in the average battery power by around 9.2%–64.1% for different driving cycles. There are two major benefits to lowering the battery power: (1) the battery will have a longer cycle life with a lower charge/discharge rate; (2) the heat generated by the battery's internal resistance will be less, and therefore the extra energy used to cool down the battery could be reduced.

Figure 10 shows the simulation results chosen from a part of the UDDS driving cycle to investigate the behavior of the engine and battery under different strategies. Note that discharging is defined as a positive current. Strategy 1 optimizes the operation of the engine by minimizing the instantaneous "equivalent fuel consumption" and could lead to two special situations: (1) the engine is operating at the optimal high load while the power required for driving is relatively low; (2) the engine stops while the battery provides the total required power, which is positive. These will result in relatively large charge and discharge currents in the battery, and the engine could start and stop frequently; however, fuel economy is optimized. Under Strategy 2, the engine–generator set's output power is limited by the NVH constraint and may no longer be inside the efficient range. For example, during the time period from 180 s–185 s, the engine–generator set was running at 10 kW, since the driver released the acceleration pedal soon after the engine was on but the engine could not shut down due to the "minimum engine-on time" constraint. However, this NVH constraint can improve the drivability of the vehicle and lower the battery power. The "minimum engine-on time" constraint can also avoid overly frequent engine on/off switching. Under Strategy 3, HCCI combustion allows the engine to operate at a low load with high efficiency; thus, it brings benefits to fuel economy, SOC stability, and battery health.

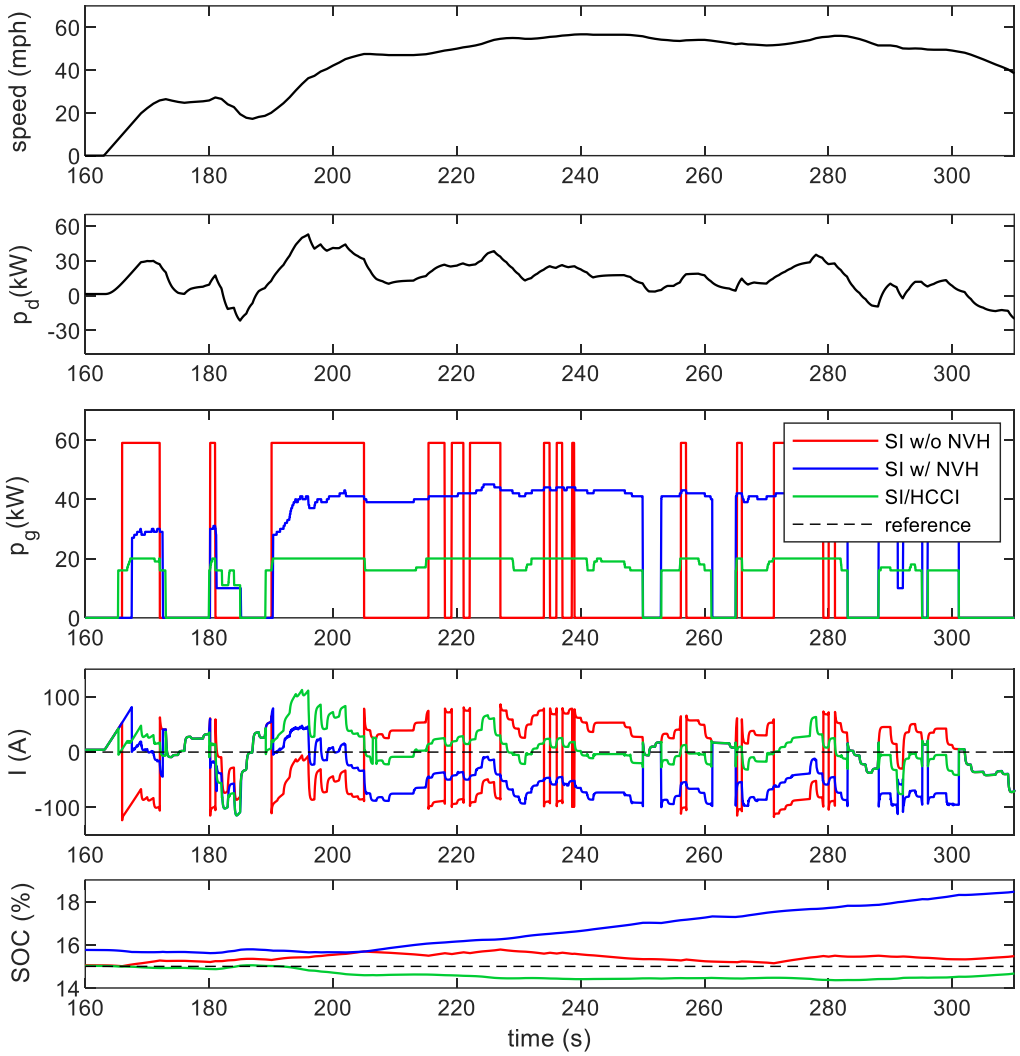


Figure 10. Simulation results under the UDDS driving cycle.

The other case is chosen from the NYCC driving cycle, reflecting urban driving conditions, as shown in Figure 11. Due to the relatively tight NVH constraint at low vehicle

speeds, the engine's optimal operating power is limited to almost below 30 kW, where it does not reach the most efficient range for SI combustion; this can explain why the average BSFC of the engine is significantly higher with NVH constraints than without them under the NYCC cycle, as shown in Table 3. On the other hand, even without considering NVH constraints, once the engine is turned on and is operating at the most efficient point, the battery will be charged at a high rate and consequently be subject to larger SOC fluctuations, while with the dual-mode combustion engine, the battery power is reduced and SOC is better sustained.

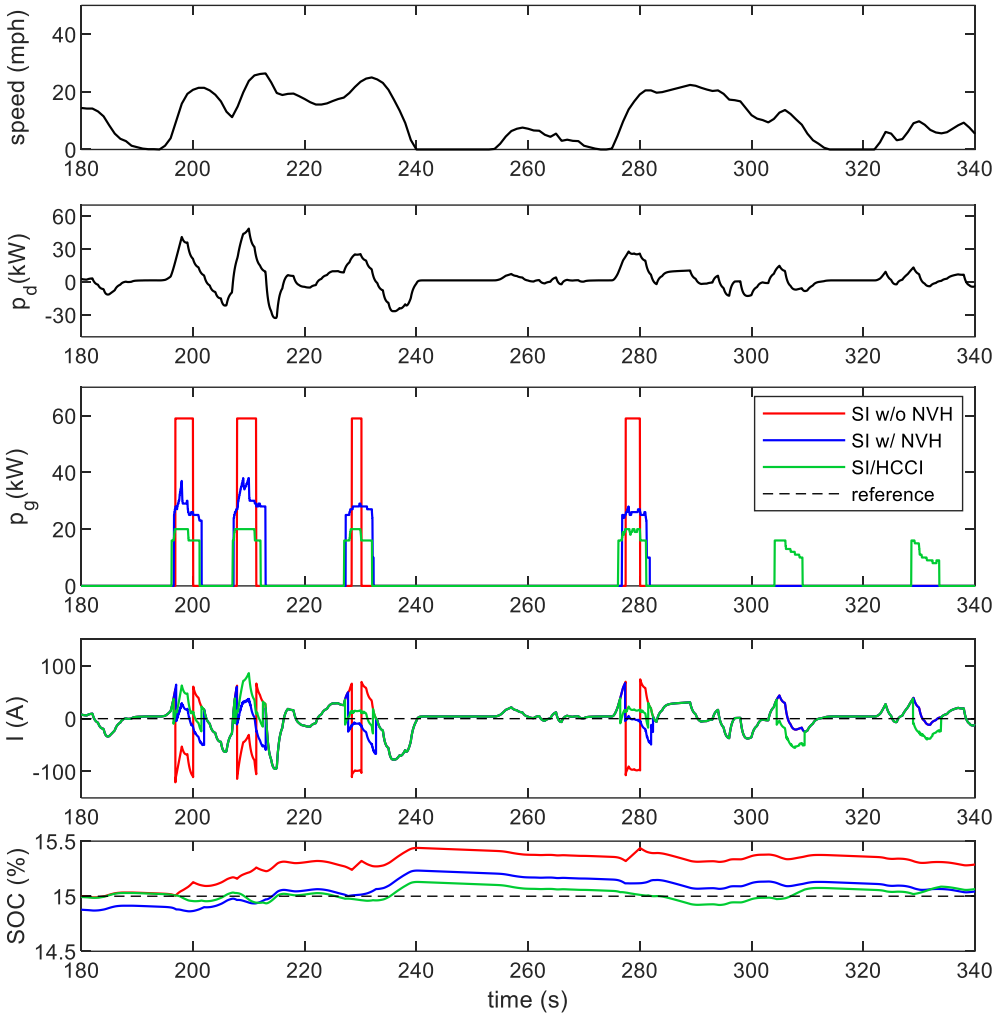


Figure 11. Simulation results under the NYCC driving cycle.

Figure 12 shows the distribution of engine operating modes under different strategies for all five testing cycles. Under Strategy 1, the EV mode without the engine on is the overwhelmingly dominant mode; this is because the global optimal engine operating power is significantly higher than the average driving load. Under Strategy 2, the engine operating power is limited by the NVH constraint and, in some of the cases, it is lower than the global optimum; therefore, the engine must have more opportunities to run to sustain the battery's SOC. Under Strategy 3, besides the increase in engine operating time, there are two detailed facts to be noted. One is that, among the five testing cycles, SI combustion only occurs in the US06 cycle, specifically at a high driving load; in all of the other four cycles, the engine only operates in the HCCI combustion mode. This shows that, based on the powertrain system configuration of this particular vehicle, it is more economical to run the engine in the HCCI mode under normal driving conditions. Only when the load power is relatively high is it better to switch to the SI mode at the global optimal point to avoid

large amounts of power being used to operate the battery, as well as to save fuel. The other fact is that, in the HWFET cycle, the engine is on for around 80% of the driving time. This is mainly due to the coincidence that the average load power is close to the optimal HCCI operating power. This can also explain why the battery loss in this case is much smaller than that under the other two strategies, as shown in Table 3.

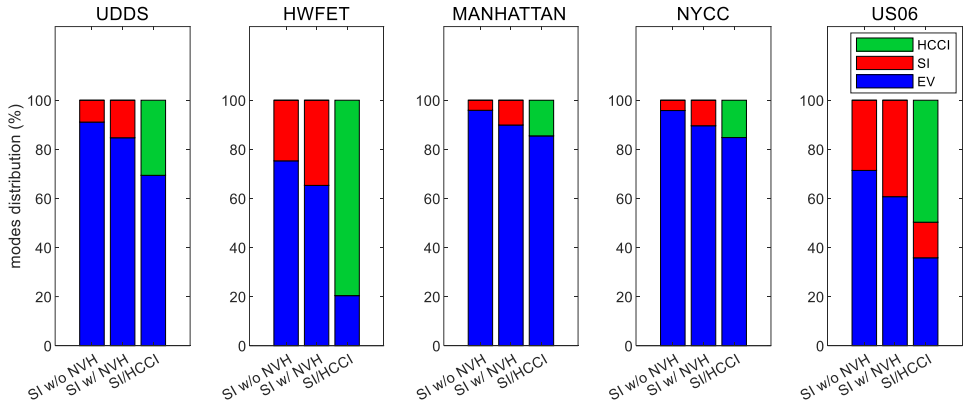


Figure 12. Distribution of engine operating modes under different strategies.

Based on the simulation results and the analysis above, it can be seen that the control parameters and operating behaviors of the engine are driving-condition-dependent. However, normally, in real-world driving, the driving conditions for a whole trip are unknown, and it is not possible to run the cycles repeatedly through a dual-loop PSO to determine the optimal EF of the ECMS. Therefore, a further investigation into the control parameters was conducted to fix an EF for online applications. From Table 2, it can be seen that there is a relationship between α and vehicle speed or load; at a lower vehicle speed, the average driving load is relatively low, and a larger α is needed to increase the opportunities to turn on the engine. This can be achieved by increasing the weight of the equivalent fuel consumption of the battery to avoid a continuous decrease in the SOC. On the contrary, a smaller α is needed at higher vehicle speeds to increase the opportunities to turn off the engine. Based on the average speed of each testing cycle and the corresponding optimal α, a vehicle-speed-based approach is applied in the final online control algorithm, as shown in Figure 13.

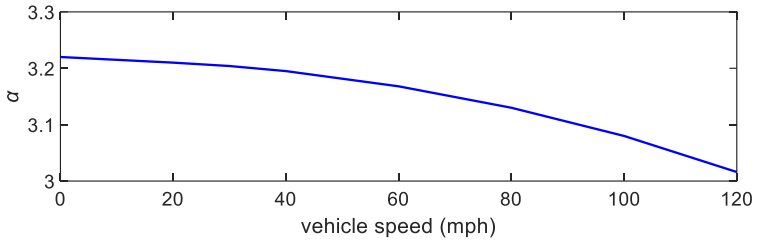


Figure 13. Variable α with respect to the vehicle speed.

The parameter β in the EF is used for SOC tracking. The simulation shows that, with a fixed α in a certain driving cycle, a larger β can obtain a smaller SOC fluctuation, and worsen the fuel consumption as a trade-off. For the convenience of control, a constant value of 0.025 is chosen for β in the real-time application.

Finally, the WLTC driving cycle is chosen to validate the proposed ECMS with a predetermined EF and a single-loop PSO algorithm. The result is shown in Figure 14. It can be seen that, during the low-speed, medium-speed, and high-speed periods, the engine is always operating in HCCI combustion mode, and the engine operation time increases as the vehicle speed becomes higher. In the last period of the cycle, which is the ultra-high-speed period, the mode switch between SI and HCCI combustion appears, and SI combustion

occurs during periods of aggressive acceleration and high-speed cruise. The SOC tracking error is less than ±1% for most of the time. Although the SOC is lower than the target value at high vehicle speeds, the tracking error is small at the end of the cycle and at any time when the vehicle stops.

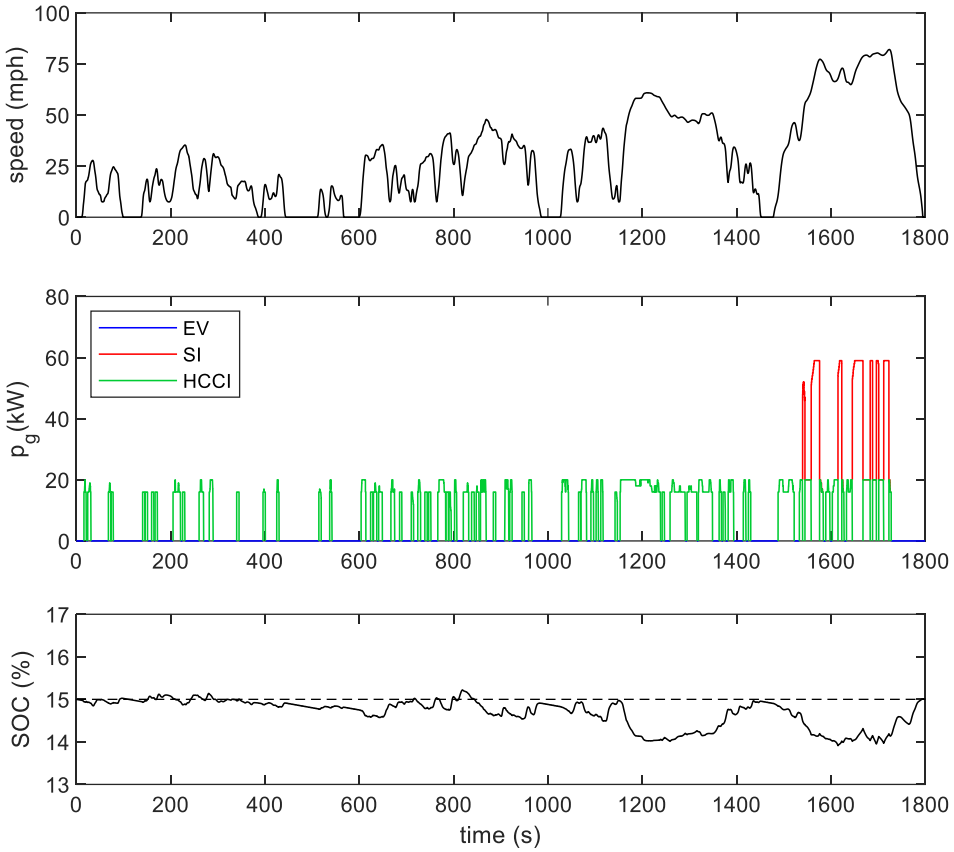


Figure 14. Simulation results under the WLTC driving cycle.

5. Conclusions

In this study, an energy management strategy based on the ECMS was proposed for a plug-in SHEV equipped with an SI/HCCI dual-mode combustion engine. The intention was to improve fuel economy under the NVH constraints of the ICE at low vehicle speeds. A dual-loop PSO was designed to obtain an optimal EF during offline optimization and solve the ECMS problem for online applications. A simulation based on a well-calibrated Simulink model of the target SHEV powertrain system was performed for different driving cycles to investigate the impact of NVH constraints on fuel economy and evaluate the improvement achieved by the proposed algorithm. The main findings of this study are as follows:

- The dual-mode engine and the proposed EMS can reduce fuel consumption by 1.3%–9.9% for different driving cycles on the target SHEV. The largest improvement was achieved in the MANHATTAN and NYCC cycles, which represent traffic conditions. This is due to a significant improvement in fuel efficiency when using the HCCI mode in comparison with the SI mode at a low load range under NVH constraints.
- The dual-mode combustion option offers two optimal engine operating ranges: a high load in SI mode or a low load in HCCI mode. When combined with the proposed ECMS, the engine can achieve an average BSFC close to the global optimal value under all the testing driving cycles. In the cycles with lower vehicle speeds, the HCCI mode is the dominant mode; as the vehicle speed increases, the engine has more opportunities

to operate in the SI mode, such as via the US06 cycle and the ultra-high-speed period of the WLTC cycle.

- The dual-mode engine and the proposed EMS also reduced the average battery power by 9.2% to 64.1% for different driving cycles. This will further reduce the battery heat losses and the future power needed for battery cooling, as well as extend the lifespan of the battery.

Future work will focus on the implementation of the proposed control strategy in the real-time hardware-in-the-loop (HIL) simulation and experimental validation on the test bench.

Author Contributions: Conceptualization, S.Z. and H.W.; methodology, S.Z.; modeling and coding, C.Y., Z.O. and S.Z.; simulation and validation, Z.O. and X.W.; writing—original draft preparation, S.Z.; writing—review and editing, H.W. All authors have read and agreed to the published version of the manuscript.

Funding: This research was supported by the project "Modeling and Control of New Energy Vehicle Powertrain Systems" funded by Shenzhen Technology University with grant number 2018010801007.

Data Availability Statement: Simulation and experiment data which do not reflect confidential information about the target engine and vehicle are available from the corresponding author upon reasonable request.

Acknowledgments: We would like to thank our lab technicians and students who supported the experiments related to this paper.

Conflicts of Interest: The authors declare no conflicts of interest.

References

1. Serrao, L.; Onori, S.; Rizzoni, G. A Comparative Analysis of Energy Management Strategies for Hybrid Electric Vehicles. *J. Dyn. Syst. Meas. Control* **2011**, *133*, 031012. [CrossRef]
2. Li, S.G.; Sharkh, S.M.; Walsh, F.C.; Zhang, C.N. Energy and Battery Management of a Plug-In Series Hybrid Electric Vehicle Using Fuzzy Logic. *IEEE Trans. Veh. Technol.* **2011**, *60*, 3571–3585. [CrossRef]
3. Ehsani, M.; Gao, Y.; Longo, S.; Ebrahimi, K. Hybrid Electric Vehicles. In *Modern Electric, Hybrid Electric, and Fuel Cell Vehicles*, 3rd ed.; CRC Press: Boca Raton, FL, USA, 2018; pp. 113–117.
4. Peng, J.; He, H.; Xiong, R. Rule Based Energy management strategy for a series–parallel plug-in hybrid electric bus optimized by dynamic programming. *Appl. Energy* **2016**, *185*, 1633–1643. [CrossRef]
5. Zhu, Y.; Li, X.; Liu, Q.; Li, S.; Xu, Y. Review article: A comprehensive review of energy management strategies for hybrid electric vehicles. *Mech. Sci.* **2022**, *13*, 147–188. [CrossRef]
6. Ali, A.M.; Söffker, D. Towards Optimal Power Management of Hybrid Electric Vehicles in Real-Time: A Review on Methods, Challenges, and State-OF-The-Art Solutions. *Energies* **2018**, *11*, 476. [CrossRef]
7. Jalil, N.; Kheir, N.A.; Salman, M. A rule-based Energy Management Strategy for a Series Hybrid Vehicle. In Proceedings of the American Control Conference, Albuquerque, NM, USA, 4–6 June 1997.
8. Cheng, Y.; Chen, K.; Chan, C.; Bouscayrol, A.; Cui, S. Global modeling and control strategy simulation for a hybrid electric vehicle using electrical variable transmission. In Proceedings of the 2008 IEEE Vehicle Power and Propulsion Conference, Harbin, China, 3–5 September 2008.
9. Hou, C.; Xu, L.; Wang, H.; Ouyang, M.; Peng, H. Energy management of plug-in hybrid electric vehicles with unknown trip length. *J. Frankl. Inst.* **2014**, *352*, 500–518. [CrossRef]
10. Kum, D.; Peng, H.; Bucknor, N.K. Optimal Control of Plug-in HEVs for Fuel Economy Under Various Travel Distances. *Ifac Proc. Vol.* **2010**, *43*, 258–263. [CrossRef]
11. Chen, B.; Wu, Y.; Tsai, H. Design and analysis of power management strategy for range extended electric vehicle using dynamic programming. *Appl. Energy* **2014**, *113*, 1764–1774. [CrossRef]
12. Zou, Y.; Liu, T.; Sun, F.; Peng, H. Comparative study of dynamic programming and Pontryagin's minimum principle on energy management for a parallel hybrid electric vehicle. *Energies* **2013**, *6*, 2305–2318. [CrossRef]
13. Liu, T.; Yu, H.; Guo, H.; Qin, Y.; Zou, Y. Online Energy Management for Multimode Plug-in Hybrid Electric Vehicles. *IEEE Trans. Ind. Inform.* **2018**, *15*, 4352–4361. [CrossRef]
14. Chen, S.; Wu, C.; Hung, Y.; Chung, C. Optimal strategies of energy management integrated with transmission control for a hybrid electric vehicle using dynamic particle swarm optimization. *Energy* **2018**, *160*, 154–170. [CrossRef]
15. Paganelli, G. Design and Control of a Parallel Hybrid Car with Electric and Thermal Powertrain. Ph.D. Thesis, University of Valenciennes, Valenciennes, France, 1999.

16. Serrao, L.; Onori, S.; Rizzoni, G. ECMS as a realization of Pontryagin's minimum principle for HEV control. In Proceedings of the 2009 American Control Conference, Hyatt Regency Riverfront, Jacksonville, FL, USA, 10–12 June 2009.
17. Enang, W.; Bannister, C. Robust proportional ECMS control of a parallel hybrid electric vehicle. *Proc. Inst. Mech. Eng. Part D J. Automob. Eng.* **2017**, *1*, 99–119. [CrossRef]
18. Chen, Z.; Liu, Y.; Ye, M.; Zhang, Y.; Li, G. A survey on key techniques and development perspectives of equivalent consumption minimisation strategy for hybrid electric vehicles. *Renew. Sustain. Energy Rev.* **2021**, *151*, 111607. [CrossRef]
19. Sivertsson, M. Adaptive control using map-based ECMS for a PHEV. In Proceedings of the 2012 Workshop on Engine and Powertrain Control, Simulation and Modeling, Rueil-Malmaison, France, 23–25 October 2012.
20. Sun, C.; Sun, F.; He, H. Investigating adaptive-ECMS with velocity forecast ability for hybrid electric vehicles. *Appl. Energy* **2016**, *185*, 1644–1653. [CrossRef]
21. Xie, S.; Hu, X.; Qi, S.; Lang, K. An artificial neural network-enhanced energy management strategy for plug-in hybrid electric vehicles. *Energy* **2018**, *163*, 837–848. [CrossRef]
22. Shen, D.; Han, J.; Karbowski, D.; Rousseau, A. Data-Driven Design of Model Predictive Control for Powertrain-Aware Eco-Driving Considering Nonlinearities Using Koopman Analysis. *IFAC-PapersOnLine* **2022**, *55–24*, 117–122. [CrossRef]
23. Gupta, S.; Shen, D.; Karbowski, D.; Rousseau, A. Koopman Model Predictive Control for Eco-Driving of Automated Vehicles. In Proceedings of the 2022 American Control Conference, Atlanta, GA, USA, 8–10 June 2022.
24. Nugroho, S.A.; Chellapandi, V.P.; Borhan, H. Vehicle Speed Profile Optimization for Fuel Efficient Eco-Driving via Koopman Linear Predictor and Model Predictive Control. In Proceedings of the 2024 American Control Conference, Toronto, ON, Canada, 8–12 July 2024.
25. Hall, J.; Marlok, H.; Bassett, M.; Warth, M. Analysis of Real World Data from a Range Extended Electric Vehicle Demonstrator. *SAE Int. J. Altern. Powertrains* **2015**, *4*, 20–33. [CrossRef]
26. Zhao, H. Motivation, definition and history of HCCI/CAI engines. In *HCCI and CAI Engines for the Automotive Industry*, 1st ed.; Woodhead Publishing: Cambridge, UK, 2007; pp. 6–36.
27. Jade, S.; Larimore, J.; Hellstrom, E.; Stefanopoulou, A.G.; Jiang, L. Controlled Load and Speed Transitions in a Multicylinder Recompression HCCI Engine. *IEEE Trans. Control Syst. Technol.* **2015**, *23*, 868–881. [CrossRef]
28. Nueesch, S.; Stefanopoulou, A.G. Multimode combustion in a mild hybrid electric vehicle. Part 1: Supervisory control. *Control Eng. Pract.* **2016**, *57*, 99–110. [CrossRef]
29. Ahn, K.; Whitefoot, J.; Babajimopoulos, A.; Ortiz-Soto, E.; Papalambros, P.Y. Homogeneous charge compression ignition technology implemented in a hybrid electric vehicle: System optimal design and benefit analysis for a power-split architecture. *Proc. Inst. Mech. Eng. Part D J. Automob. Eng.* **2012**, *227*, 87–98. [CrossRef]
30. Solouk, A.; Tripp, J.; Shakiba-Herfeh, M.; Shahbakhti, M. Fuel consumption assessment of a multi-mode low temperature combustion engine as range extender for an electric vehicle. *Energy Convers. Manag.* **2017**, *148*, 1478–1496. [CrossRef]
31. Zhang, H.; Fan, Q.; Liu, S.; Li, S.E.; Huang, J.; Wang, Z. Hierarchical energy management strategy for plug-in hybrid electric powertrain integrated with dual-mode combustion engine. *Appl. Energy* **2021**, *304*, 117869. [CrossRef]
32. Zhang, Y.; Wu, H.; Mi, S.; He, Z.; Qian, Y.; Lu, X. Optimization of intelligent charge compression ignition engine in hybrid electric powertrain by adaptive equivalent consumption management strategy. *Energy* **2024**, *307*, 132585. [CrossRef]
33. Ambühl, D.; Sciarretta, A.; Onder, C.; Christopher, H.; Guzzella, L.; Sterzing, S.; Mann, K.; Kraft, D.; Küsell, M. A Causal Operation Strategy for Hybrid Electric Vehicles based on Optimal Control Theory. In Proceedings of the 4th Symposium Hybrid Vehicles and Energy Management, Braunschweig, Germany, 14–15 February 2007.

Disclaimer/Publisher's Note: The statements, opinions and data contained in all publications are solely those of the individual author(s) and contributor(s) and not of MDPI and/or the editor(s). MDPI and/or the editor(s) disclaim responsibility for any injury to people or property resulting from any ideas, methods, instructions or products referred to in the content.